Harvesting the Vibration Energy with $BaTiO_3$@Graphene for the Piezocatalytic Degradation of Methylene Blue

Tian Hou[1], Fang Cao[1], Meilin Li[2], Jinlong Wang[1,*] and Lingling Lv[3]

[1]*School of Resources and Environmental Engineering, Wuhan University of Technology, Wuhan 430070, China*

[2]*Department of Chemistry, University of Connecticut, Storrs, CT 06269-3060, USA*

[3]*Ordos Institute of Environmental Science, Ordos, China*

Abstract: Piezocatalysis is a newly advanced oxidation process (AOP) which can be triggered by mechanical force to generate electric field, and then drives free charge carriers to participate redox reactions. In this work, reduced graphene oxide (rGO) is integrated with the widely used barium titanate (BTO) to regulate the surface free charges of composites. The piezocatalytic activity of integrated composite (BTO@rGO) is strongly related with the mass ratio of BTO and rGO. Driven by ultrasonic force, BTO@rGO can completely decompose methylene blue (MB) within 120 min when the mass ratio of BTO to rGO is 2:1, showing the best activity comparing with samples of other mass ratios (10:1, 5:1, and 1:1). The introduction of graphene facilitates the interface charge transfer to BTO, which is proved by peak shift information of Raman and X-ray photoelectron spectroscopy (XPS). The generated hydroxyl radical (·OH) is the active species participating in MB oxidation. This work not only gives a clear understanding of interface electron transfer mechanism but also sheds light on the construction of well-performed piezocatalysts.

Keywords: Barium titanate, Graphene, Piezocatalyst, Free charges, Methylene blue.

1. INTRODUCTION

Piezocatalysis is a catalytic effect driven by the stress-induced electricity of piezoelectric crystallites. When a physical force is applied to its surface, the position of asymmetric atoms in the material is deviated from the original position, resulting in the generation of positive and negative charges on the opposite surface to overcome polarization. The separated charges will then participate in the chemical reactions via generated free radicals [1]. Up to now, piezocatalysis has been widely used in the area of organic pollutants degradation, electrochemical polymerization, hydrogen generation and heavy metal collection [2].

Barium titanate (BTO) is a commonly used piezocatalyst. Its piezocatalytic avtivity is decided by two parameters: geometric structure and surface free charges concentration. Hong *et al*. [1] reported BTO nanowires can stimulate water decomposition to produce hydrogen driven by ultrasonic vibration. The easy deformation facilitates the charges separation, which benefits for the subsequent reaction. Similar phenomena were also observed on nanorod BTO catalyst [3]. In addition, surface free charges concentration is another important parameter. BTO micron sized particle without optimized geometric shape also exhibits enhanced 4-chlorophenol degradation activity. It is because calcination at 800 °C enhances carrier concentration on the surface of BTO [4]. Meanwhile, Lin *et al*. [5] reported that the surface modification of precious metals (such as Ag, Pt, Au, Ru and Pd) can effectively improve the catalytic activity of piezoelectric catalysts. Free charges concentration can also be regulated by introducing defects [6]. In addition, constructing an integrated composite between an electron donor and an electron acceptor can also regulate electronic abundance at contacted interface. However, the limit of this concept for an interacting system has not yet been well established.

Graphene is a two-dimensional material constructed by carbon sp^2 hybridization. It shows unique thermal, electrical, optical and mechanical properties [7]. Integrating graphene with nanomaterials can alter the physical and chemical properties of the composite materials. Wang *et al*. [8] reported the introduction of graphene into MnO_2 can enhance the electronic density around the Mn atom on the surface of MnO_2 due to the orbital hybridization between the π electron of graphene and the d orbits of MnO_2. Ji *et al*. [9] found similar phenomena in the system of MnO_x and carbon nanotubes. The presence of graphene promoted the transfer of electrons from carbon nanotube to MnO_x, thus accelerating the chemical reaction process. From this perspective, the introduction of graphene into BTO system might improve the piezocatalytic performance of BTO.

*Address correspondence to this author at the School of Resources and Environmental Engineering, Wuhan University of Technology, Wuhan 430070, China; E-mail: wjl16@whut.edu.cn

E-ISSN: 2311-8741/20

In this work, the reduced graphene oxide (rGO) and BTO were integrated. The structure and interface electron transfer characteristics of the composite were explored.

Methylene blue (MB) was chosen as the characteristic pollutant to study the piezocatalytic performance of the composite under the ultrasonic force. At the same time, the influencing factors, such as the ultrasonic power, the pH value of the reaction solution, the catalyst dosing amount were also discussed. Finally, the main reactive species were discussed and a possible mechanism were proposed.

2. EXPERIMENTAL

2.1. Sample Preparation

First, BTO powder was prepared by calcination method [4]. The purchased barium titanate powder was placed in a tubular furnace, annealed in air at 800 °C for 2 h. Then, a certain amount of graphene oxide powder and prepared BTO were both added into 60 mL deionized water and ultrasonically dispersed for 2 min until the solution was uniformly mixed. After that, 30 mL of anhydrous ethyl alcohol was added, and quickly stirred. The mixture was transferred to a Teflone sealed autoclave (100 mL) and maintained at 160 °C for 24 h. The precipitate was centrifuged and dried overnight at 60 °C for 12 h. The black composite materials with mass ratios were obtained. For comparison, pure BTO and rGO were also synthesized.

2.2. Characterization Methods

The crystal structure of different samples was tested by X-ray diffraction (XRD; D/Max-Red, Rigaku) using Cu *Kα* radiation. The morphologies and microstructure of different samples were characterized by scanning electron microscopy (SEM; Merlin Compact 61-78, Zeiss), high resolution transmission electron microscopy (HR-TEM; JEM-2100F, JEOL). Raman was conducted using a Renishaw Micro-Raman Spectroscopy (Via plus, Renishaw) with a laser of 514 nm. The surface element state of samples was determined by X-ray photoelectron spectra (XPS; Escalab 250Xi, Thermo Fisher). The active species existed in MB degradation process were measured by electron paramagnetic resonance (EPR; 220 SE, Bruker). 5,5-dimethyl-1-pyrroline N-oxide (DMPO) is used as radical trapping reagent.

2.3. The Evaluation of Piezocatalytic Activity

Typically, 8 mg of sample is dispersed in 100 mL of 5 $mg \cdot L^{-1}$ MB aqueous solution to form a suspension. The ultrasonic vibration is created by an ultrasonic cleaner (KX-1620, China) with a frequency of 40 kHz and a power of 100 W. Samples are taken periodically (every 20 min) and centrifuged in a 4900r/min centrifuge (TD5A-WS, China). The concentration of MB is measured by a Shimadzu UV-3600 spectrophotometer. In addition, experiments under continuous stirring without ultrasonic vibration are also carried out for comparison. The influential parameters such as pH and ultrasonic power are tested. The pH is adjusted by HCl and NaOH.

3. RESULTS AND DISCUSSION

3.1. Structure Characterizations

Figure **1** shows the XRD patterns of BTO, rGO and BTO@rGO composites. Pure BTO displays obvious diffraction peaks at 2*θ* of 21.99°, 31.56°, 38.87°, 45.20°, 50.89°, 56.09° and 65.77°, which are indexed to the crystallite planes of (100), (110), (111), (200), (210), (211) and (220) in a tetragonal BTO (JCPDS card NO. 05-0626) [10, 11]. The diffraction peak at 31.56 ° in BTO single component is more sharp than other peaks, indicating that the crystal surface (110) is the main exposed crystal surface. In addition, a broad diffraction peak around 25° is the characteristic peak of rGO [12-14]. From the XRD patterns of BTO@rGO composites, the main peak is BTO phase while the diffraction peak of rGO is not obvious. The images of three different samples are also shown in Figure **1**. In the XRD patterns of BTO@rGO samples with different mass ratios (10:1, 5:1, 2:1, 1:1), the main peaks of all BTO@rGO samples are still the diffraction patterns of BTO, indicating that the compositing process does not affect the crystal structure of BTO. With the increase of

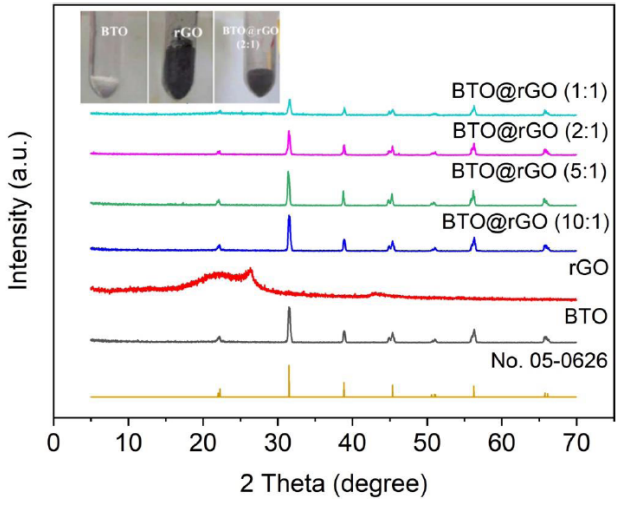

Figure 1: XRD patterns of BTO, rGO, and BTO@rGO with different mass ratios (10:1, 5:1, 2:1, 1:1).

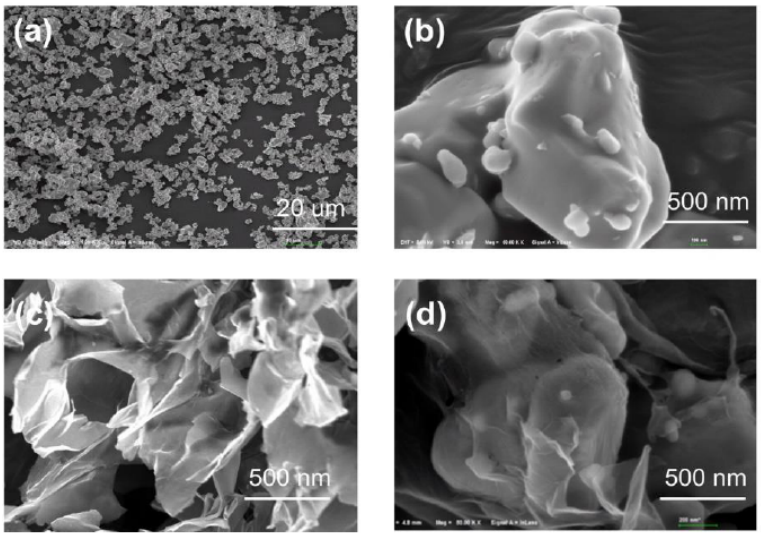

Figure 2: SEM images of (**a**, **b**) BTO, (**c**) rGO, and (**d**) BTO@rGO (2:1).

the composite ratio, the peak at 21.99° gradually widens, which further proves the successful preparation of BTO@rGO composite.

Figure **2** shows the SEM images of different samples. The size of BTO particle is around 500 nm (Figure **2b**), and there are many small particles on its surface, which may be fragments formed in the calcination process. Figure **2c** shows the morphology of rGO. rGO has a sheet like structure. The easy deformation of the layer structure provides the possibility for the integration with BTO particles. In Figure **2d**, for BTO@rGO sample, BTO is completely wrapped in rGO. Such a structure might improve the electronic transfer at the contact interface and improve the piezoelectric catalytic performance of the material.

The morphology of BTO from TEM images (Figure **3a, b**) is similar with that of SEM, further indicating the uniform morphology. In Figure **3c**, the lattice fringe of

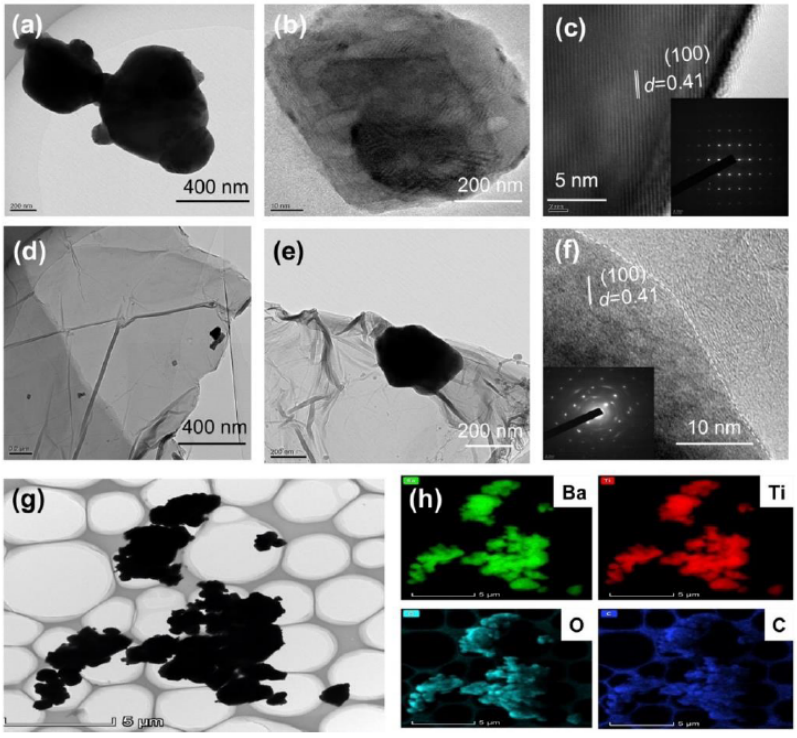

Figure 3: TEM of (**a-c**) BTO, (**d**) rGO, (**e, f**) BTO@rGO, and element mapping of (**g, h**) BTO@rGO (2:1).

BTO with a spacing of 0.41nm is observed, which corresponds to (100) crystal facet [15]. Moreover, the clear diffraction spots in the SAED pattern of BTO indicates its single crystal structure. The TEM image of rGO is transparent (Figure **3d**), indicating its ultrathin structure, which can be easily wrapped with BTO particles (shown in Figure **3e**). In Figure **3f**, the dashed part is the contact interface between BTO and rGO. The electron diffraction ring in the selected area indicates that the composite exhibits property of polycrystalline structure. This might because the interference of the rGO background, further indicating the strong interaction between BTO and rGO. In addition, the element mappings of BTO@rGO composite are also illustrated (Figure **g, h**). The enrichment of C, Ba, Ti, O occurs at the same position, indicating the two materials are closely integrated.

The interface charge transfer process is systematically discussed by Raman and XPS. In Figure **4a**, two strong peaks between 1330 cm^{-1} and 1590 cm^{-1} in the spectra of rGO and BTO@rGO are observed. The peaks at 1335 or 1344 cm^{-1} and 1589 or 1597 cm^{-1} belong to band D and G respectively, and band D represents the existence of defect or disorder carbon, while band G represents the existence of graphite carbon [16]. The intensity ratio (I_D/I_G) indicates the relative abundance of sp^3 hybrid carbon atoms, corresponding to the defects in graphene lattice. The intensity ratio (I_D/I_G) of the two samples (rGO and BTO@rGO) is almost equal, indicating the introduction of BTO will not change the structure of rGO. The G-band shift in carbon matrix composites is related to the electron transfer between carbon and other compounds [8, 17]. The blue shift from 1589 to 1597 cm^{-1} was observed, indicating the electron transfer from rGO to BTO [9]. There is no obvious barium titanate peak in the dotted frame, which may be due to the strong peak of rGO. Figure **4b** shows the Ba 3d XPS curve. The binding energy of BTO and BTO@rGO is 778.5 and 778.3 eV, respectively [18]. The lower binding energy of Ba 3d in BTO@rGO indicates the BTO@rGO have more free electrons on the surface, further proving the possible electron transfer. Figure **4c** shows the Ti 2p XPS curve. The binding energies of Ti 2p XPS in two samples are same (457 eV) [19]. The introduction of graphene has ignorable effect on the electron structure of Ti atom. From the TEM image in Figure **3f**, (100)

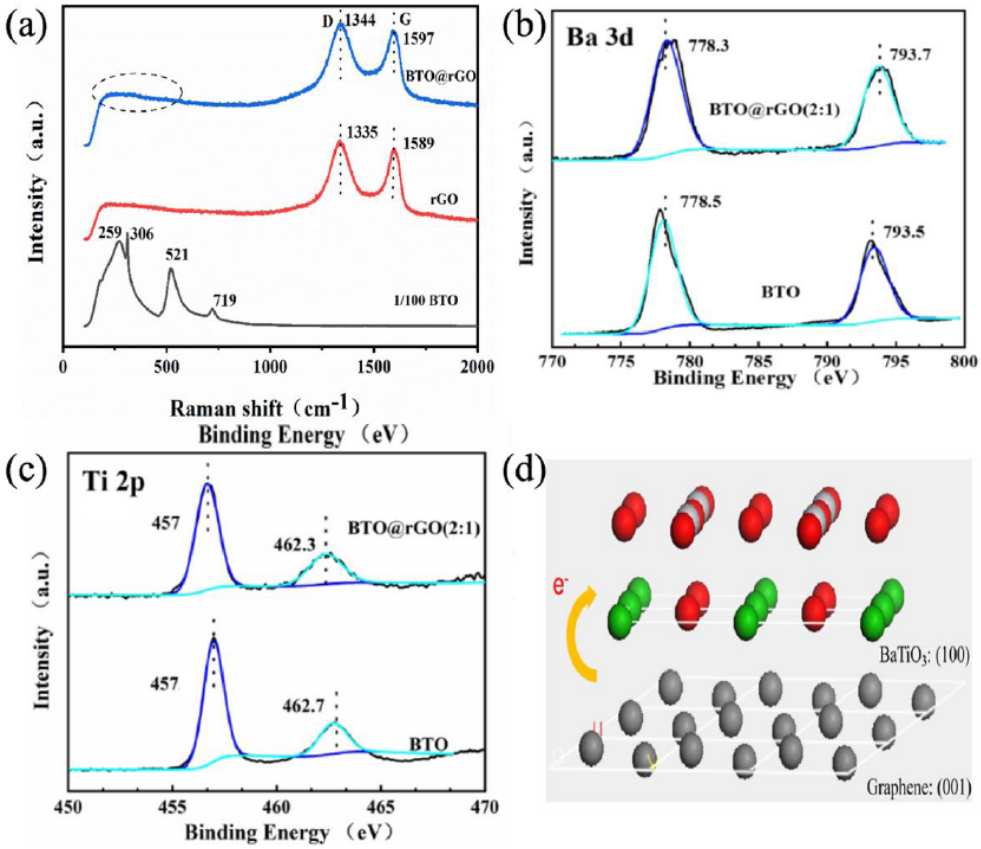

Figure 4: (**a**) Raman shift of BTO, rGO, and BTO@rGO (2:1) samples. (**b, c**) XPS curves of Ba 3d and Ti 2p. (**d**) Schematic diagram of electron transfer between BTO and rGO. The green, light gray, red, and dark gray balls are Ba, Ti, O, and C atoms, respectively.

crystal facet is observed at contacted interface. Ba and O atoms are exposed at (100) facet, which can hybrid with C atom (Figure **4d**), resulting the electron transfer from graphene to BTO.

3.2. Piezocatalytic Activity

To evaluate the piezocatalytic performance, the degradation of MB is carried out under different conditions. In Figure **5a**, the ultrasonic vibration without a catalyst has no effect on the MB molecule. The MB removal ratio is 20% and 36% using BTO or rGO separately. Once rGO is integrated with BTO, the MB removal ratios are all increased. When the ratio is 2:1, the removal ratio of MB can be reached as high as 98% within 120 min. However, when the content of rGO is further increased, the piezocatalytic activity starts to decrease, which is because of the reduction of active component (BTO). In addition, the dynamic analysis is also given (Figure **5b**). According to the Langmuir-Hinshelwood model, the piezocatalytic processes can be fit to pseudo-first-order kinetics ($-\ln(C/C_0) = k\,t$), where k is the rate constant; C_0 and C is the initial and dynamic concentration of MB solution; t is the reaction time. By calculating the corresponding reaction rate constant k, we can obtain the k value of BTO@rGO (2:1) (0.028 min^{-1}), while the k value of pristine BTO is 0.002 min^{-1}. The k value of the composite BTO@rGO is 14 times to that of the pristine BTO. The introduction of graphene promotes the piezocatalytic performance.

Figure **6a** shows the piezocatalytic experiment under different ultrasonic conditions (120, 180, 240, and 300 W). Ultrasonic energy can lead to the acoustic cavitation, resulting in the formation, growth and collapse of cavitation bubbles in a liquid [20]. With the collapse of bubble, the partial pressure will cause the deformation of piezocatalyst. In this work, ultrasonic power of 300 W exhibits the best MB decomposition activity. In addition, the effect of pH value of MB solution was also discussed (Figure **6b**). When the pH value of the solution is 9, the degradation rate is about 50 %. When the pH value is neutral, the degradation rate increases to about 60 %. When the pH value is 1, the degradation rate is close to 100 %. The results show that strong acid condition is helpful to the degradation of methylene blue, while weak acid or alkaline condition is not conducive to the reaction. The point of zero charge of BTO is near the pH of 3 [21]. This means that the surface charge of BTO is positively charged when the pH is below 3. At higher pH values, repulsion may occur between the negatively charged MB and the surface of BTO, inhibiting MB adsorption. In Figure **6c**, the dosage of BTO@rGO was also discussed. When the catalyst dosage is 0.04 $g{\cdot}L^{-1}$, the removal ratio of MB is 50 %. With the continuous increase of catalyst dosage, the removal ration of MB gradually enhanced. However, when the dosage is further increase (from 0.08 to 0.3 $g{\cdot}L^{-1}$), the removal efficiency no longer increases. At last, the stability of BTO@rGO was tested (Figure **6d**). After 4 times recycles, the removal ratio of MB still maintains at 78%, indicating its reusable property.

3.3. Piezocatalytic Mechanism

The free radical species during the piezocatalytic process are measured. In Figure **7a**, the superoxide radicals ($\cdot O_2^-$) and hydroxyl radicals ($\cdot$OH) are trapped in DMPO methanol and DMPO water solutions. No radicals can be detected on rGO sample. $\cdot O_2^-$ and $\cdot$OH radicals can be both observed on BTO and BTO@rGO samples, indicating the ultrasonicaiton triggers free radical generation. The intensity of $\cdot O_2^-$ and $\cdot$OH signals is much higher on BTO@rGO than that of BTO,

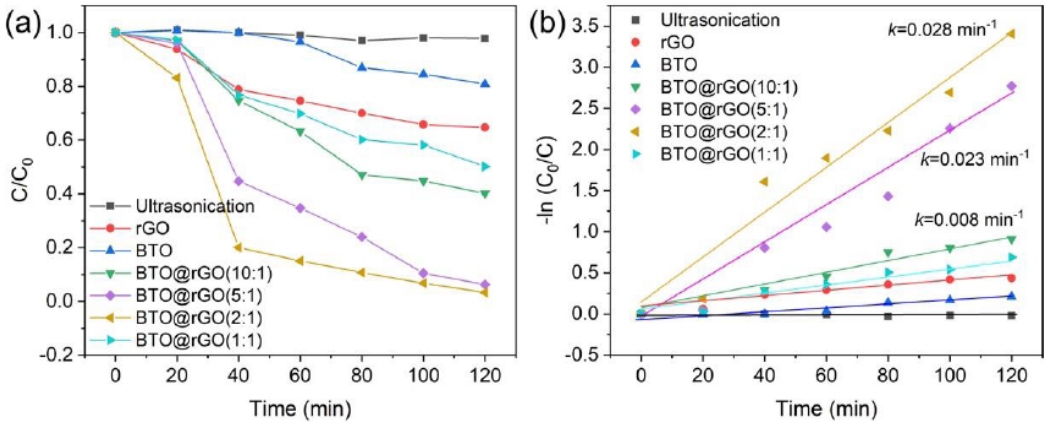

Figure 5: (**a**) MB removal ratio, and (**b**) dynamitic curves over different samples.

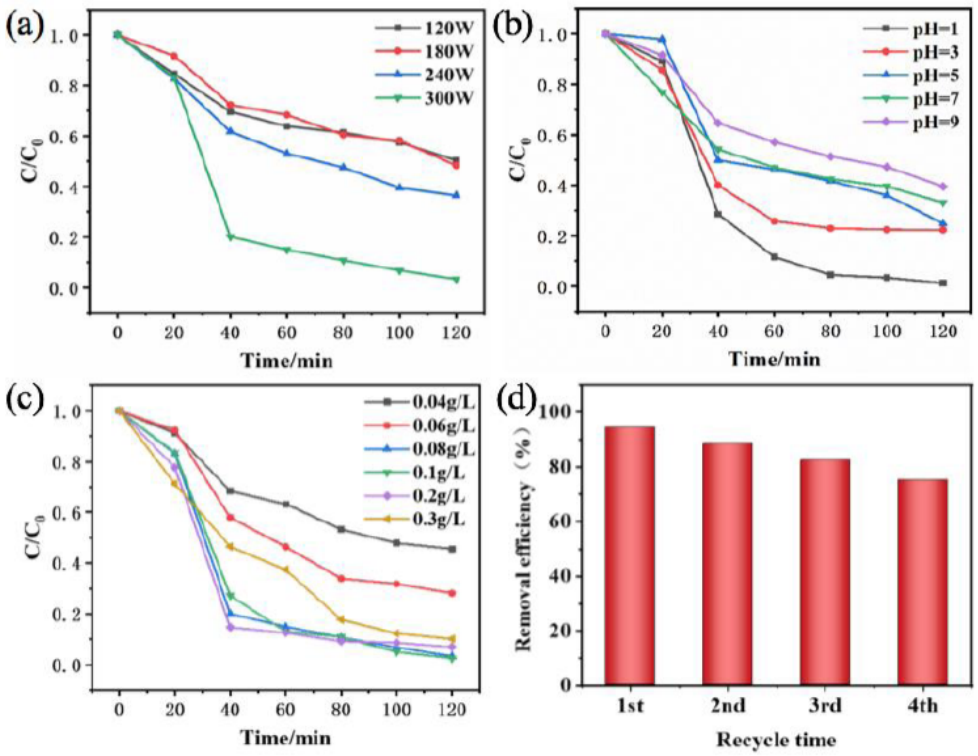

Figure 6: The effect of (**a**) ultrasonic power, (**b**) pH, (**c**) catalyst dosage, (**d**) stability over BTO@rGO (2:1) sample. (Catalyst amount: 8 mg; MB concentration: 5 mg·L^{-1}).

indicating the introduction of rGO enhances the piezocatalytic activity. As discussed above, free charges transfer from rGO to BTO at contacted interface, resulting in abundant free charges which can be involved in the reaction with O_2 or H_2O with the generation of free radicals. In Figure **7b**, the changes of $\cdot O_2^-$ monitored with the time. When ultrasonication is applied, the intensity of $\cdot O_2^-$ increases with the time (before 2 min). However, when the reaction time is prolonged, no accumulated $\cdot O_2^-$ is detected in our system. It means that the generated $\cdot O_2^-$ might be transformed into other species. For ·OH, it accumulated with the time, and no attenuation is observed (Figure **7c**). To further confirm the roles of all species, benzoquinone (BQ), isopropyl alcohol (IPA), and sodium oxalate ($Na_2C_2O_4$), are used as $\cdot O_2^-$, ·OH, and h^+ scavengers, respectively (Figure **7d**). The MB removal ratio of BQ and IPA captured experiment decreases to 39% and 26% in 120 min comparing with the pristine experiment (98%). However, the $Na_2C_2O_4$ captured experiment exhibits negligibly reduced activity. This result indicates $\cdot O_2^-$ and ·OH are mainly active species in MB decomposition reaction. Combined with the EPR experiment in Figure **7b**, the attenuation of $\cdot O_2^-$ with the reaction time might be its transformation into ·OH [4, 6]. Chemical reaction equations are listed for better understanding equations (1) - (5):

$$BTO@rGO \xrightarrow{Ultrasonicp\ power} e^- + h^+ \quad (1)$$

$$OH^- + h^+ \rightarrow \cdot OH \quad (2)$$

$$O_2 + e^- \rightarrow \cdot O_2^- \quad (3)$$

$$\cdot O_2^- + H^+ \rightarrow \cdot OOH \rightarrow H_2O_2 \rightarrow \cdot OH \quad (4)$$

$$\cdot OH + MB \rightarrow Intermediates + CO_2 + H_2O \quad (5)$$

From the above discussion, ·OH is the active species participating in MB oxidation and it is mainly from $\cdot O_2^-$ transformation. It is reported ·OH radicals can attack C-S=C groups of thionine ring, inducing the opening of central heterocylic ring of phenothiazine structure. In addition, the dedimethylation or dedimethylamino reaction also occurs. Specifically, two symmetrical dimethylaminos groups on thionine ring can be successively hydroxylated by replacement of dimethylamino groups. The imino-group groups in central rings can be oxidized to aniline and finally transformed to nitrate anions [22-24]. Through breaking C-S=C, C-N=C, N-$(CH_3)_2$, H_2N-C_6H_5 bonds, MB molecular will be decomposed into smaller fragments towards total degradation to CO_2.

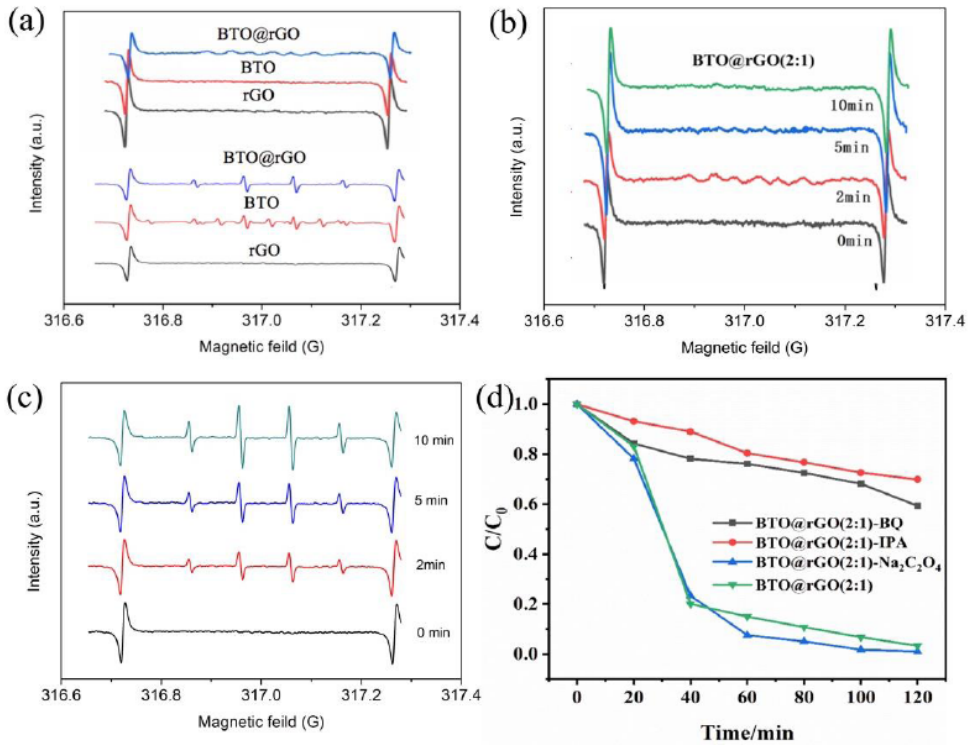

Figure 7: EPR spectra of BTO, rGO, and BTO@rGO under ultrasonication (2 min): (**a**)·O_2^- and ·OH radicals trapped by DMPO + CH_3OH. (**b**, **c**) radical changes with the time over BTO@rGO sample. (**d**) MB degradation ability of BTO@rGO with respect to various scavengers: BQ→·O_2^-, IPA→·OH, $Na_2C_2O_4$→h^+ (Catalyst amount: 8 mg; MB concentration: 5 mg·L^{-1}).

Based on the above analysis, the possible degradation mechanism is proposed as shown in Figure **8**. More free charges are generated due to the electron transfer from graphene to BTO, which can be involved in the free radical generation. The ultrasonic vibration provides the power to trigger the deformation of BTO, which can result in the separation of negative and positive charges. In this system, ·OH radicals are the main species responsible for MB decomposition. Most of ·OH radical comes from the transformation of ·O_2^- rather than h^+.

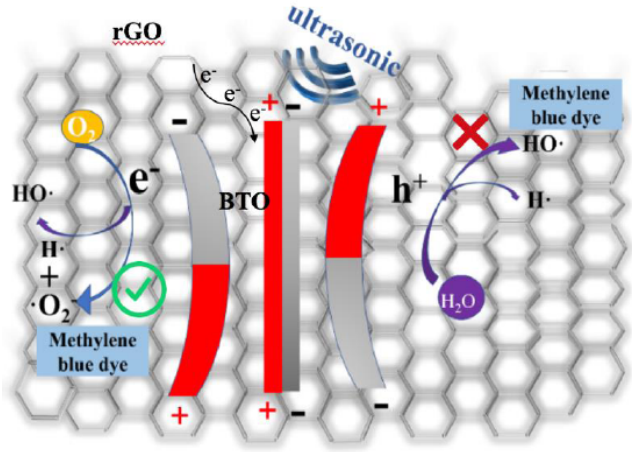

Figure 8: Mechanism diagram of piezocatalytic reaction.

4. CONCLUSIONS

In this study, BTO@rGO composite were successfully synthesized. Graphene is an electron-rich material, and the electrons on its surface can be partly transferred to BTO via constructing contacted interface. As a result, the content of free charges BTO can be enhanced, which is good for its piezocatalytic activity. Driven by ultrasonic power, more free radicals such as ·O_2^- and ·OH radicals are generated on the integrated composites, which are good for the piezocatalytic activity. The ·OH radical is dominated in the entire piezocatalytic process and plays the key role in MB decomposition.

ACKNOWLEDGEMENTS

This work is financially supported by State Key Joint Laboratory of Environment Simulation and Pollution Control (No. 17K08ESPCT).

REFERENCES

[1] Hong KS, Xu H, Konishi H, Li X. Piezoelectrochemical effect: a new mechanism for azo dye decolorization in aqueous solution through vibrating piezoelectric microfibers. Journal of Physical Chemistry C 2012; 116(24): 13045-13051. https://doi.org/10.1021/jp211455z

[2] Liang Z, Yan C, Rtimi S, Bandara J. Piezoelectric materials for catalytic/photocatalytic removal of pollutants: recent

advances and outlook. Applied Catalysis B: Environmental 2019; 241: 256-269. https://doi.org/10.1016/j.apcatb.2018.09.028

[3] Wu J, Qin N, Bao D. Effective enhancement of piezocatalytic activity of $BaTiO_3$ nanowires under ultrasonic vibration. Nano Energy 2018; 45: 44-51. https://doi.org/10.1016/j.nanoen.2017.12.034

[4] Lan S, Feng J, Xiong Y, Tian S, Liu S, Kong L. Performance and mechanism of piezoecatalytic degradation of 4-chlorophenol: finding of effective piezo-edechlorination. Environmental Science & Technology 2017; 51: 6560-6569. https://doi.org/10.1021/acs.est.6b06426

[5] Lin E, Wu J, Qin N, Yuan B, Bao D. Silver modified barium titanate as a highly efficient piezocatalyst. Catalysis Science & Technology 2018; 8: 4788-4796. https://doi.org/10.1039/C8CY01127C

[6] Nie Q, Xie Y, Ma J, Wang J, Zhang G. High piezo–catalytic activity of ZnO/Al_2O_3 nanosheets utilizing ultrasonic energy for wastewater treatment. Journal of Cleaner Production 2019; 242: 118532. https://doi.org/10.1016/j.jclepro.2019.118532

[7] Zhou Y, Zhang X, Zhang Q, Dong F, Wang F, Xiong Z. Role of graphene on the band structure and interfacial interaction of Bi_2WO_6/graphene composites with enhanced photocatalytic oxidation of NO. Material Chemistry A 2014; 2(39): 16623-16631. https://doi.org/10.1039/C4TA03762F

[8] Wang J, Zhang G, Zhang P. Graphene-assisted photothermal effect on promoting catalytic activity of layered MnO_2 for gaseous formaldehyde oxidation. Applied Catalysis B: Environmental 2018; 239: 77-85. https://doi.org/10.1016/j.apcatb.2018.08.008

[9] Ji J, Fang Y, He L, Huang H. Efficient catalytic removal of airborne ozone at ambient condition over manganese oxides immobilized on carbon nanotubes. Catalysis Science & Technology 2019; 9(15): 4036-4046. https://doi.org/10.1039/C9CY00762H

[10] Wu J, Xu Q, Lin E, Yuan B, Bao D. Insights into the role of ferroelectric polarization in piezocatalysis of nanocrystalline $BaTiO_3$. ACS Applied Materials & Interfaces 2018; 10(21): 17842-17849. https://doi.org/10.1021/acsami.8b01991

[11] Lin E, Qin N, Wu J, Yuan B, Kang Z, Bao, D. $BaTiO_3$ nanosheets and caps grown on TiO_2 nanorod arrays as thin-film catalysts for piezocatalytic applications. ACS Applied Materials & Interfaces 2020; 12(12): 14005-14015. https://doi.org/10.1021/acsami.0c00962

[12] Pan M, Zhang C, Wang J. Multifunctional Piezoelectric Heterostructure of $BaTiO_3$@Graphene: Decomplexation of Cu-EDTA and Recovery of Cu. Environmental Science &Technology 2019; 53(14): 8342-8351. https://doi.org/10.1021/acs.est.9b02355

[13] Wen B, Cao M, Lu M, Cao W, Shi H, Liu J, Wang X et al. Reduced graphene oxides: Light-weight and high-efficiency electromagnetic interference shielding at elevated temperatures. Advanced Material 2014; 26: 3484-3489. https://doi.org/10.1002/adma.201400108

[14] Muthumariyappan A, Rajaji U, Chen SM, Kumar BN, Chen TW, Ramalingam RJ. Sonochemical synthesis of perovskite-type barium titanate nanoparticles decorated on reduced graphene oxide nanosheets as an effective electrode material for the rapid determination of ractopamine in meat samples. Ultrasonics Sonochemistry 2019; 56: 318-326. https://doi.org/10.1016/j.ultsonch.2019.04.005

[15] Wu J, Qin N, Bao D. Effective enhancement of piezocatalytic activity of $BaTiO_3$ nanowires under ultrasonic vibration. Nano Energy 2018; 44-51. https://doi.org/10.1016/j.nanoen.2017.12.034

[16] Wu JB, Lin ML, Cong X, Liu HN, Tan PH. Raman spectroscopy of graphene-based materials and its applications in related devices. Chemical Society Reviews 2018; 10: 1039. https://doi.org/10.1039/C6CS00915H

[17] Yu J, Ma T, Liu S. Enhanced photocatalytic activity of mesoporous TiO_2 aggregates by embedding carbon nanotubes as electron-transfer channel. Physical Chemistry Chemical Physics, 2011, 13, 3491-3501 https://doi.org/10.1039/C0CP01139H

[18] Yuan B, Wu J, Qin N, Lin E, Bao DH. Enhanced piezocatalytic performance of (Ba, Sr) TiO_3 nanowires to degrade organic pollutants. ACS Applied Nano Material 2018; 1: 5119-5127. https://doi.org/10.1021/acsanm.8b01206

[19] Xu X, Wu Z, Xiao L, Ji Y, Ma J, Wang F. Strong piezo-electro-chemical effect of piezoelectric $BaTiO_3$ nanofibers for vibration-catalysis. Journal of Alloys and Compounds 2018: 915-921. https://doi.org/10.1016/j.jallcom.2018.05.279

[20] Wang P, Ji W, Li M, Zhang G, Wang J. $Bi_{25}VO_{40}$ microcube with step surface for visible light photocatalytic reduction of Cr(VI): enhanced activity and ultrasound assisted regeneration. Ultrasonics Sonochemistry 2017; 289-297. https://doi.org/10.1016/j.ultsonch.2017.03.016

[21] Hou D, Jian G, Hu Y, Zheng Y, Gong S, Liu H. Electrophoretic deposition of multiferroic $BaTiO_3/CoFe_2O_4$ bilayer films. Materials Chemistry & Physics 2011; 127(1-2): 316-321. https://doi.org/10.1016/j.matchemphys.2011.02.004

[22] Nguyen CH, Fy CC, Juang RS. Degradation of methylene blue and methyl orange by palladium-doped TiO_2 photocatalysis for water reuse: Efficiency and degradation pathways. Journal of Cleaner Production 2018; 202: 413-427. https://doi.org/10.1016/j.jclepro.2018.08.110

[23] Su S, Liu Y, Liu X, Jin W, Zhao Y. Transformation pathway and degradation mechanism of methylene blue through β-FeOOH@GO catalyzed photo-Fenton-like system. Chemosphere 2019; 218: 83-92. https://doi.org/10.1016/j.chemosphere.2018.11.098

[24] Wolski L, Ziolek M. Insight into pathways of methylene blue degradation with H_2O_2 over mono and bimetallic Nb, Zn oxides. Applied Catalysis B: Environmental 2018; 224: 634-647. https://doi.org/10.1016/j.apcatb.2017.11.008

Received on 10-07-2020 Accepted on 05-08-2020 Published on 18-08-2020

DOI: https://doi.org/10.12974/2311-8741.2020.08.8